Acta Crystallographica Section F
Structural Biology Communications
ISSN 2053-230X

Structure of *Mycobacterium smegmatis* Eis in complex with paromomycin

Kyoung Hoon Kim,[a] Doo Ri An,[a] Hye Jin Yoon,[a] Jin Kuk Yang[b] and Se Won Suh[a,c]*

[a]Department of Chemistry, College of Natural Sciences, Seoul National University, Seoul 151-742, Republic of Korea, [b]Department of Chemistry, College of Natural Sciences, Soongsil University, Seoul 156-743, Republic of Korea, and [c]Department of Biophysics and Chemical Biology, College of Natural Sciences, Seoul National University, Seoul 151-742, Republic of Korea

Correspondence e-mail: sewonsuh@snu.ac.kr

Received 7 May 2014
Accepted 29 July 2014

PDB reference: Eis, complex with paromomycin, 4qb9

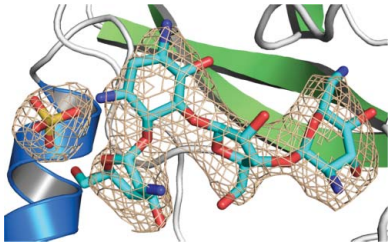

The *Rv2416c* gene of *Mycobacterium tuberculosis* (*Mtb*) encodes the enhanced intracellular survival (Eis) protein that enhances intracellular survival of the pathogen in host macrophages during infection. The *Mtb* Eis protein is released into the cytoplasm of the phagocyte during intracellular infection and modulates the host immune response. It also contributes to drug resistance by acetylating multiple amine groups of aminoglycosides. Interestingly, the nonpathogenic *M. smegmatis* (*Msm*) contains a homologous *eis* gene (MSMEG_3513). The overall structures of *Mtb* Eis and *Msm* Eis are highly similar to each other, reflecting the high level (58%) of amino-acid sequence identity between them. Both *Mtb* Eis and *Msm* Eis are active as aminoglycoside acetyltransferases, while only *Mtb* Eis functions as an N^{ε}-acetyltransferase to acetylate Lys55 of dual-specificity protein phosphatase 16 (DUSP16)/mitogen-activated protein kinase phosphatase 7 (MKP-7), leading to the suppression of host immune responses. Here, the crystal structure of *Msm* Eis in the paromomycin-bound form is reported, revealing detailed interactions between an aminoglycoside antibiotic and *Msm* Eis. The crystal structure of *Msm* Eis in the paromomycin-bound form has been determined at 3.3 Å resolution. This work provides potentially useful information for structure-guided discovery of Eis inhibitors as a novel antituberculosis drug against drug-resistant *Mtb*.

1. Introduction

Tuberculosis remains one of the world's most destructive bacterial infectious diseases. *Mycobacterium tuberculosis* (*Mtb*), the causative agent of tuberculosis, is a highly successful human pathogen. It infects one third of the global population and claims nearly two million lives every year (Dye & Williams, 2010). It has the ability to persist in the form of a long-term asymptomatic infection, referred to as latent tuberculosis (Lin & Flynn, 2010). Latent tuberculosis becomes activated when the body's immune system is weakened. As a result, tuberculosis is the major cause of death among immunocompromised AIDS patients (Getahun *et al.*, 2010). Despite efforts to ensure proper drug dosages and patient compliance with drug regimens, multidrug-resistant and extensively drug-resistant strains of *Mtb* have emerged (Chiang *et al.*, 2010). This makes the search for targets of new antituberculosis drugs urgent. *Mtb* has evolved a number of very effective intracellular survival strategies (Meena & Rajni, 2010) and is able to survive and multiply within human macrophages (Dahl *et al.*, 2001). Since intracellular survival plays a central role in the pathogenesis of *Mtb* (Wei *et al.*, 2000), the mycobacterial proteins responsible for intracellular survival remain a priority for the development of new antituberculosis drugs.

The *Rv2416c* gene in *Mtb* H37Rv, designated *eis* (enhanced intracellular survival), was found to enhance intracellular survival of *M. smegmatis* (*Msm*) in the human macrophage-like cell line U-937 (Wei *et al.*, 2000). The *Mtb* Eis protein is produced during human tuberculosis infection and is released into the culture medium (Dahl *et al.*, 2001). It has been shown that the sigma factor SigA binds the *eis* promoter in the W-Beijing strain of *Mtb* and that activation of the *eis* gene correlates with increased SigA levels and enhanced intracellular survival (Wu *et al.*, 2009). Treatment of T cells with Eis modulates extracellular signal-regulated kinase 1/2 (ERK1/2), the JAK pathway and the production of tumour necrosis factor α (TNF-α) and

interleukin 4 (IL-4) (Lella & Sharma, 2007). *Mtb* Eis has been shown to suppress host innate immune defences by negatively modulating inflammation, autophagy and cell death in a redox-dependent manner (Shin *et al.*, 2010). It also contributes to drug resistance by acetylating multiple amine groups of aminoglycosides (Chen *et al.*, 2011). Interestingly, the nonpathogenic *Msm* contains a homologous *eis* gene (MSMEG_3513). A high level (58%) of amino-acid sequence identity exists between the Eis proteins from *Mtb* and *Msm*. As expected, their overall structures are highly similar to each other (Kim *et al.*, 2012). We showed that both the *Mtb* Eis and *Msm* Eis proteins are active as aminoglycoside acetyltransferases (Kim *et al.*, 2012). However, they differ in the aminoglycoside substrate preference and in the number of acetylated amine groups per aminoglycoside (Chen *et al.*, 2012). We also showed that only *Mtb* Eis functions as an N^{ε}-acetyltransferase to acetylate Lys55 of dual-specificity protein phosphatase 16 (DUSP16)/mitogen-activated protein kinase phosphatase 7 (MKP-7), a JNK-specific phosphatase, leading to the suppression of host immune responses (Kim *et al.*, 2012).

Paromomycin is an aminoglycoside antibiotic; it inhibits bacterial protein synthesis by binding to 16S ribosomal RNA. Many aminoglycosides contain a 2-deoxystreptamine part substituted at different positions by amino sugars. Paromomycin is an example of the 4,5-disubstituted subclass, while tobramycin belongs to the 4,6-disubstituted subclass (Fig. 1). Previously, we showed that the acetyltransferase activity of *Msm* Eis towards paromomycin is higher than that of *Mtb* Eis (Kim *et al.*, 2012). Here, we have determined the crystal structure of *Msm* Eis in complex with paromomycin to reveal the detailed interactions between *Msm* Eis and paromomycin and to allow a comparison of its binding mode with that of tobramycin by *Mtb* Eis (Houghton *et al.*, 2013). This study provides potentially useful information for structure-guided discovery of Eis inhibitors as novel antituberculosis drugs against drug-resistant *Mtb*.

Table 1
Data-collection and refinement statistics.

Values in parentheses are for the highest resolution shell.

Data-collection statistics	
Protein	*M. smegmatis* Eis
Data set	Paromomycin complex
Resolution range (Å)	30.0–3.30 (3.36–3.30)
X-ray source	BL-5C, Pohang Light Source
X-ray wavelength (Å)	1.0000
Space group	$P2_12_12_1$
a, b, c (Å)	107.27, 126.54, 236.64
α, β, γ (°)	90, 90, 90
Total/unique reflections	89672/49506
Completeness (%)	95.4 (92.0)
Mean $I/\sigma(I)$	22.1 (6.98)
$R_{\rm merge}$† (%)	17.7 (55.9)
Refinement statistics	
Resolution range (Å)	15.0–3.30
$R_{\rm work}/R_{\rm free}$‡ (%)	15.1/23.4
No. of protein residues	2412
No. of sulfates	6
No. of paromomycins	6
Mean B factor (Å^2)	
Protein	48.9
Sulfate	81.9
Paromomycin	53.0
R.m.s. deviations from ideal geometry	
Bond lengths (Å)	0.014
Bond angles (°)	1.69
Ramachandran plot	
Most favoured (%)	91.0
Allowed (%)	9.0
Generously allowed (%)	0

† $R_{\rm merge} = \sum_{hkl}\sum_i |I_i(hkl) - \langle I(hkl)\rangle|/\sum_{hkl}\sum_i I_i(hkl)$, where $I(hkl)$ is the intensity of reflection hkl, $\sum_{hkl}$ is the sum over all reflections and $\sum_i$ is the sum over i measurements of reflection hkl. ‡ $R = \sum_{hkl}||F_{\rm obs}| - |F_{\rm calc}||/\sum_{hkl}|F_{\rm obs}|$, where $R_{\rm free}$ is calculated for a randomly chosen 10% of reflections, which were not used for structure refinement, and $R_{\rm work}$ is calculated for the remaining reflections.

2. Materials and methods

2.1. Protein expression, purification and crystallization

Msm Eis was overexpressed and purified as described previously (Kim *et al.*, 2012). The purified *Msm* Eis protein was concentrated to 48.0 mg ml^{-1} in 20 m*M* Tris–HCl pH 8.5, 0.1 m*M* TCEP, 150 m*M* NaCl (1.0 m*M* monomer concentration) for crystallization using an YM10 ultrafiltration membrane (Amicon). Crystals were grown by the sitting-drop vapour-diffusion method at 297 K by mixing 1 µl protein solution and 1 µl reservoir solution. *Msm* Eis was pre-incubated with acetyl-CoA (100 m*M*) for 30 min and was then further incubated with paromomycin (50 m*M*) for a further 30 min in 20 m*M* Tris–HCl pH 8.5, 0.1 m*M* TCEP, 150 m*M* NaCl. Thick plate-shaped crystals were obtained with a reservoir solution consisting of 1.26 *M* ammonium sulfate, 100 m*M* MES pH 6.0. They grew to approximate dimensions of 0.2 × 0.2 × 0.1 mm within 2–3 d.

2.2. X-ray data collection and phasing

The crystals were flash-cooled using a cryoprotectant solution consisting of 1.26 *M* ammonium sulfate, 100 m*M* MES pH 6.0, 25%(*v*/*v*) glycerol. The crystals were soaked in 5 µl cryoprotectant solution for 10 s before being flash-cooled in liquid nitrogen. X-ray diffraction data from a crystal of paromomycin-complexed *Msm* Eis were collected at 100 K using an ADSC Quantum 315r CCD detector system (Area Detector Systems Corporation, Poway, California, USA) on BL-5C at Pohang Light Source, Republic of Korea. The crystals of paromomycin-complexed *Msm* Eis belonged to space group $P2_12_12_1$, with unit-cell parameters a = 107.27, b = 126.54, c = 236.64 Å. Six monomers are present in the asymmetric unit, giving a Matthews coefficient and solvent fraction of 2.70 Å^3 Da^{-1} and

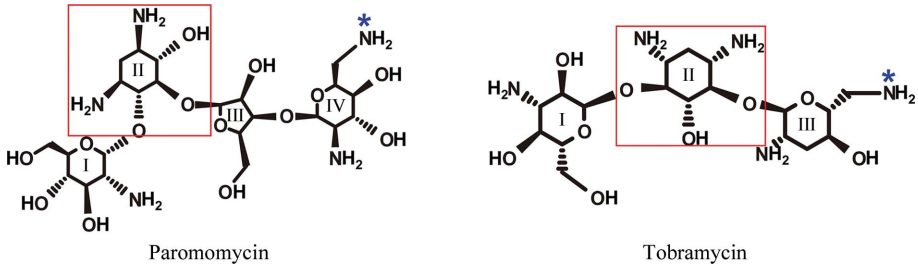

Paromomycin Tobramycin

Figure 1
Chemical structures of paromomycin and tobramycin. The 2-deoxystreptamine group is enclosed in a red box. The N64 atom of paromomycin and the N61 atom of tobramycin are marked with asterisks.

54.5%, respectively. Data-collection and phasing statistics are summarized in Table 1.

2.3. Model building and refinement

The structure was solved by molecular replacement using *Phaser* (McCoy *et al.*, 2007) in the *CCP*4 program suite (Winn *et al.*, 2011). We used the hexameric model of CoA-bound *Msm* Eis (PDB entry 3sxn; Kim *et al.*, 2012) as the search model, with the ligands and waters removed. Subsequent manual model rebuilding was carried out using *Coot* (Emsley & Cowtan, 2004) interspersed with rounds of automatic refinement by *REFMAC*5 (Murshudov *et al.*, 2011) and *PHENIX* (Adams *et al.*, 2010). The geometry of the final refined model was checked with *MolProbity* (Chen *et al.*, 2010). Refinement statistics are summarized in Table 1.

2.4. Accession code

The coordinates and structure factors for paromomycin-complexed *Msm* Eis have been deposited in the Protein Data Bank with accession code 4qb9.

3. Results and discussion

3.1. Overall quality of the structure

We have determined the crystal structure of the *Msm* Eis protein in complex with paromomycin at 3.3 Å resolution (Table 1). The refined model includes 2412 residues in six independent Eis monomers (residues 1–402 for chains *A*–*F*) and six molecules of paromomycin in the asymmetric unit. The N-terminal fusion tag is disordered in the crystal and is not visible in the electron-density map for all six

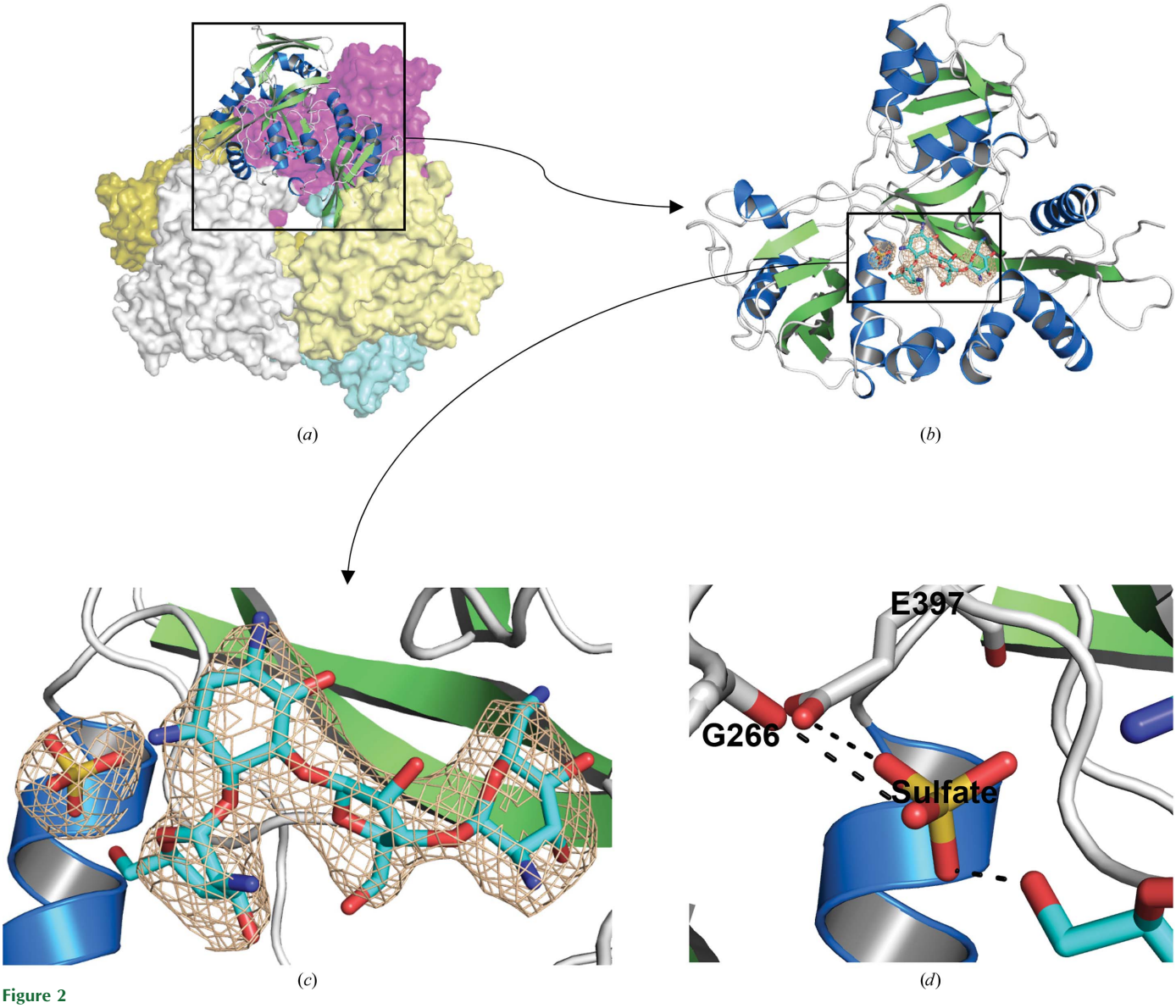

Figure 2
The crystal structure of *Msm* Eis in complex with paromomycin. (*a*) Cartoon and surface representation of the *Msm* Eis hexameric structure. Five monomers of the hexamer are shown in surface mode (coloured magenta, slate, aquamarine, pale yellow and olive) and one is shown in cartoon mode. (*b*) Cartoon representation of the monomeric structure. (*c*) The electron density of paromomycin and a sulfate ion bound to chain *A*. The wheat-coloured mesh is the simulated-annealing OMIT $F_o - F_c$ electron-density map calculated with paromomycin and the sulfate ion removed from the model (contoured at 3.0σ). (*d*) Cartoon representation of the sulfate-binding region in *Msm* Eis. Amino-acid residues and paromomycin around the sulfate ion are shown as stick models. N and O atoms are coloured blue and red, respectively. Black dotted lines denote hydrogen bonds.

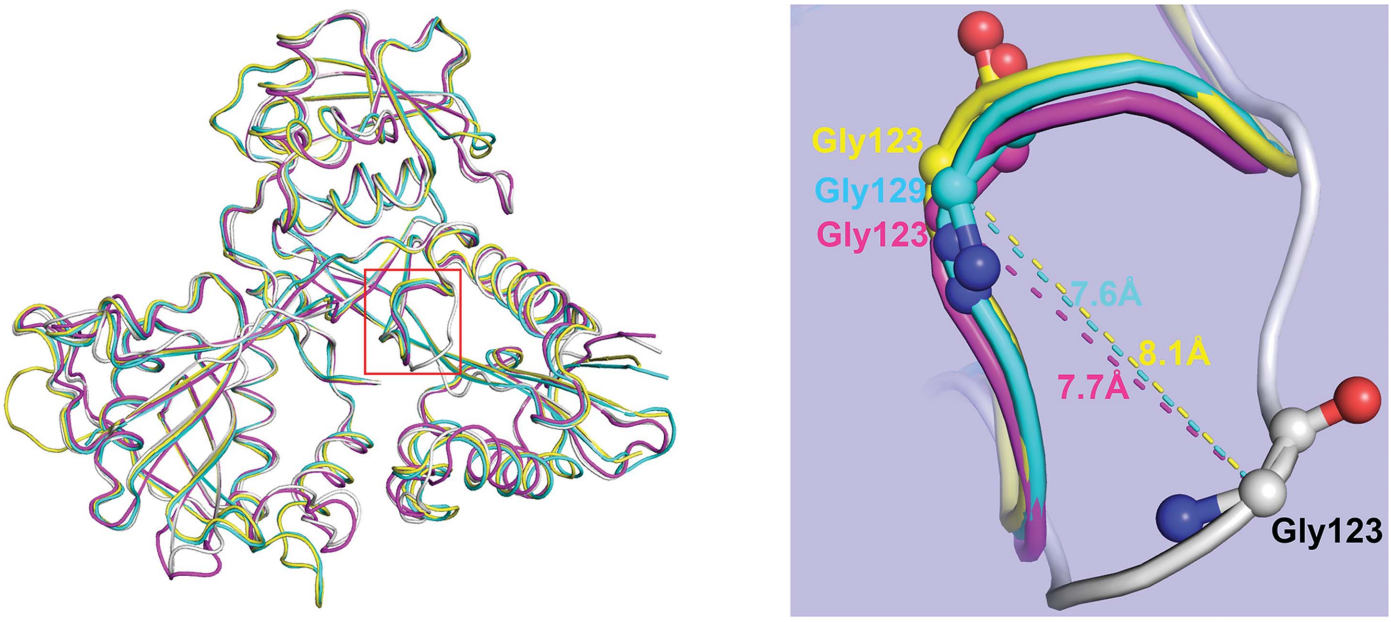

(*a*) (*b*)

Figure 3
Structural comparison of paromomycin-complexed *Msm* Eis with other *Msm* Eis and *Mtb* Eis structures. (*a*) Monomers of paromomycin-bound *Msm* Eis (grey; chain *A*), CoA/tobramycin-bound *Mtb* Eis (yellow; PDB entry 4jd6, chain *A*), CoA-bound *Msm* Eis (magenta; PDB entry 3sxn, chain *A*) and acetyl-CoA-bound *Mtb* Eis (cyan; PDB entry 3ryo, chain *A*) are superimposed. (*b*) Close-up view of the region encompassing residues Ser121–Tyr126, which are enclosed in a red box in (*a*), which displays a large structural difference. Amino-acid residues around this region are shown as stick models. Dotted lines denote the distance between C^{α} atoms.

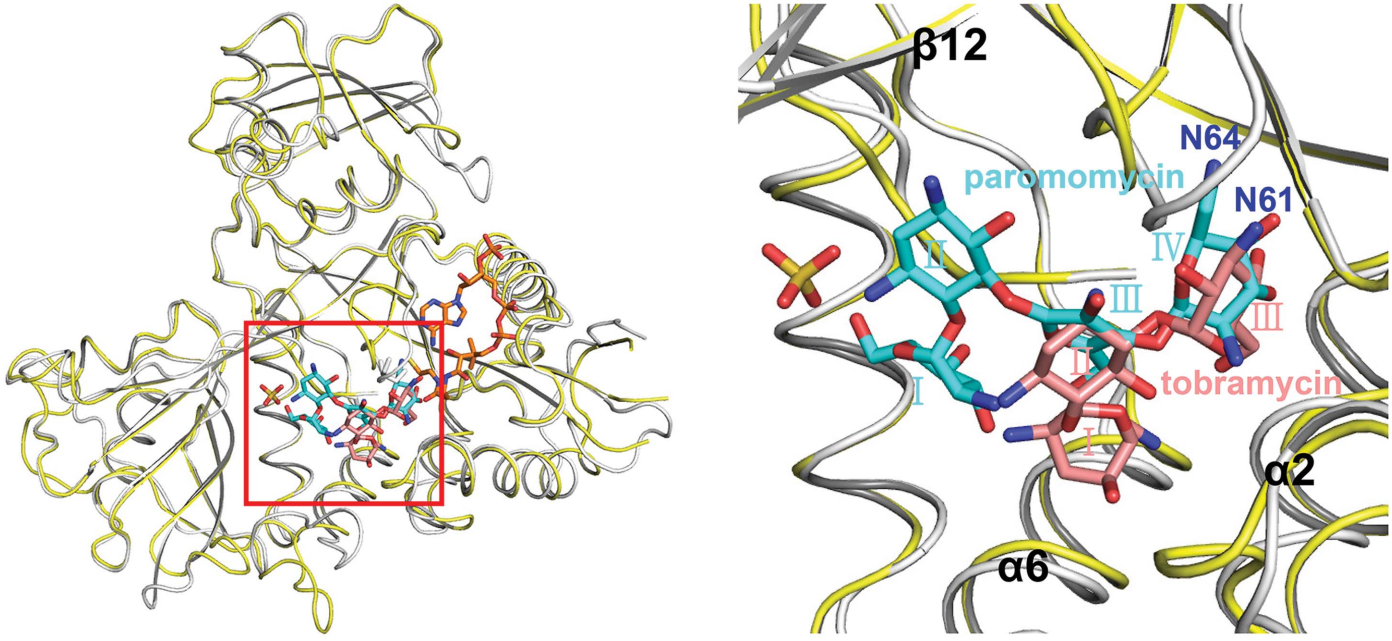

(*a*) (*b*)

Figure 4
Structural comparison of *Msm* Eis complexed with paromomycin only and *Mtb* Eis complexed with both CoA and tobramycin (binding mode *A*; Houghton *et al.*, 2013). (*a*) Monomers of paromomycin-bound *Msm* Eis (gray) and CoA/tobramycin-bound *Mtb* Eis (yellow) are superimposed. (*b*) Close-up view of the aminoglycoside-binding pocket, as indicated by a red rectangle in (*a*). Paromomycin (cyan) and tobramycin (salmon) are shown as stick models.

monomers. The six monomers of paromomycin-bound *Msm* Eis in the asymmetric unit form a hexameric molecule in the crystal (Fig. 2). They are highly similar to each other, as indicated by the small r.m.s. deviations of 0.36–0.47 Å for pairwise comparisons of chain *A* against all others over 402 C^{α} atoms. One molecule of paromomycin is noncovalently bound to the active site of each monomer and all six paromomycin molecules in the asymmetric unit are well defined by the electron density (Fig. 2 and Supplementary Fig. S1[1]). An extra electron density was observed adjacent to paromomycin and was modelled as a sulfate ion because the crystallization condition contained a high concentration of sulfate ions (Fig. 2 and Supple-

[1] Supporting information has been deposited in the IUCr electronic archive (Reference: TT5057).

mentary Fig. S1). The sulfate ion interacts with the main-chain O atoms of Gly266 (O–O distance of 3.1 Å) and Glu397 (O–O distance of 3.0 Å) and with O61 of paromomycin (O–O distance of 2.7 Å) (Fig. 2*d*). Although acetyl-CoA was present at a 100-fold excess over the *Msm* Eis monomer in the crystallization conditions, its electron density was lacking at the expected binding site.

3.2. Comparisons of paromomycin-bound *Msm* Eis with other Eis structures

To assess possible structural changes upon binding paromomycin, we superimposed paromomycin-bound *Msm* Eis (chain *A*) with other Eis structures (Figs. 3 and 4). Against CoA-bound *Msm* Eis (PDB entry 3sxn; chain *A*; Kim *et al.*, 2012), the r.m.s. deviations were 0.60–0.83 Å for monomer–monomer comparisons over 402 C^{α} atoms and 1.07 Å for a hexamer–hexamer comparison over 2412 C^{α} atoms. Notable structural differences are observed around the CoA-binding site. That is, part of the $\beta5$–$\alpha4$ loop (Ser121–Tyr126) shows a relatively large conformational difference, with a maximum C^{α} deviation of 7.7 Å at Gly123 of *Msm* Eis (Fig. 3*b*). Tyr126 is one of the key catalytic residues. Superposition of paromomycin-bound *Msm* Eis and acetyl-CoA-bound *Mtb* Eis (PDB entry 3ryo; chain *A*; Kim *et al.*, 2012) gives r.m.s. deviations of 1.4–1.7 Å for monomer–monomer comparisons over 396 C^{α} atoms and an r.m.s. deviation of 1.5–1.8 Å for a hexamer–hexamer comparison over 2376 C^{α} atoms. Ser121–Tyr126 in *Msm* Eis (corresponding to Ser127–Tyr132 in *Mtb* Eis) show a relatively large conformational difference, with a maximum C^{α} deviation of 7.6 Å at *Msm* Eis Gly123 (and *Mtb* Eis Gly129) (Fig. 3*b*). The same region shows a similarly large difference between paramomycin-complexed *Msm* Eis and CoA/tobramycin-complexed *Mtb* Eis (Houghton *et al.*, 2013), with a maximum C^{α} deviation of 8.1 Å at Eis Gly123 (Fig. 3*b*). The observed large structural differences are most likely owing to the absence of bound CoA or acetyl-CoA in our paromomycin-complexed *Msm* Eis, because the region encompassing Ser121–Tyr126 plays an important role in the interaction with CoA or acetyl-CoA (Supplementary Fig. S2; Kim *et al.*, 2012). One significant structural difference between *Msm* Eis and *Mtb* Eis is the 3_{10}-helix $\alpha6'$. It is present in both the paromomycin-bound and CoA-bound *Msm* Eis structures, but not in the apo and acetyl-CoA-complexed *Mtb* Eis structures (Supplementary Fig. S2).

In our current structure, acetyl-CoA did not bind to *Msm* Eis despite pre-incubation of the enzyme with a 100-fold excess of acetyl-CoA over the Eis monomer. The acetyl-CoA-binding site in our structure is vacant and is not even partly occupied by bound paro-

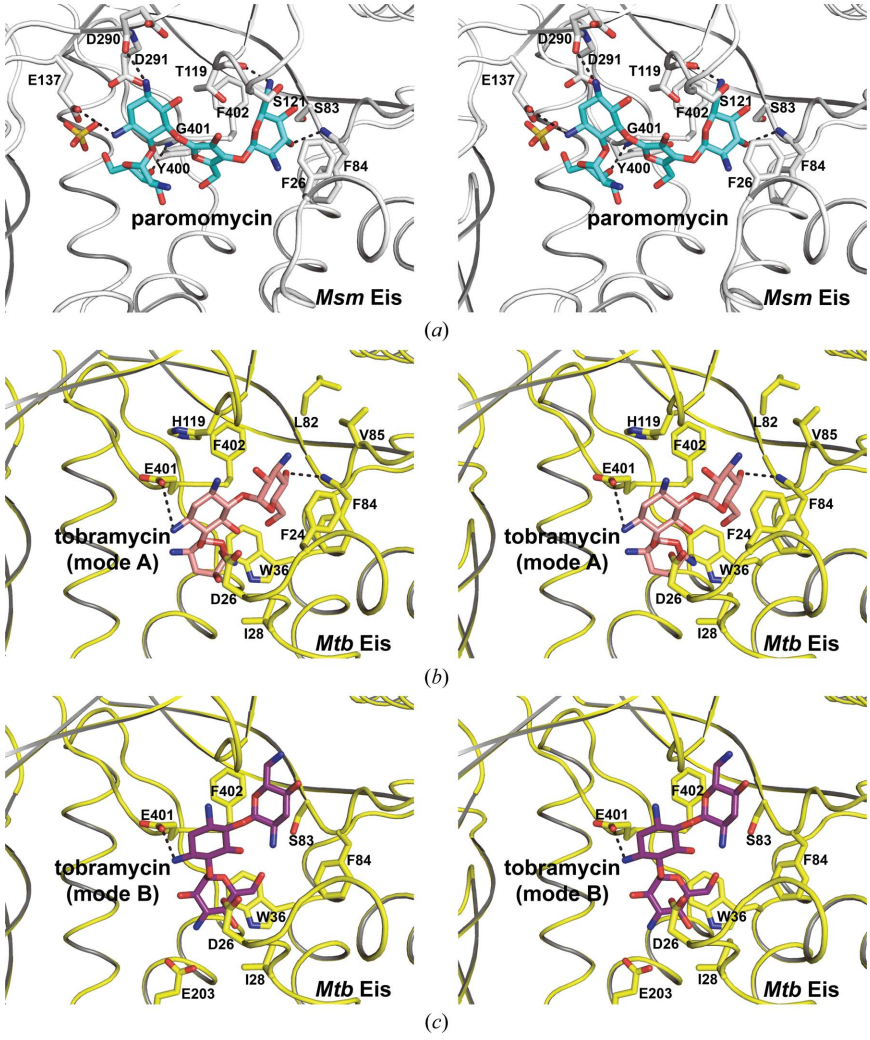

Figure 5
Stereoview of aminoglycoside binding to *Msm* Eis and *Mtb* Eis. Amino-acid residues around paromomycin or tobramycin are shown as stick models. N and O atoms are coloured blue and red, respectively. Black dotted lines denote hydrogen bonds. (*a*) Paromomycin bound to *Msm* Eis monomer (chain *A*). (*b*) Tobramycin bound to *Mtb* Eis monomer (chain *A*; mode *A*; Houghton *et al.*, 2013). (*c*) Tobramycin bound to *Mtb* Eis monomer (chain *A*; mode *B*).

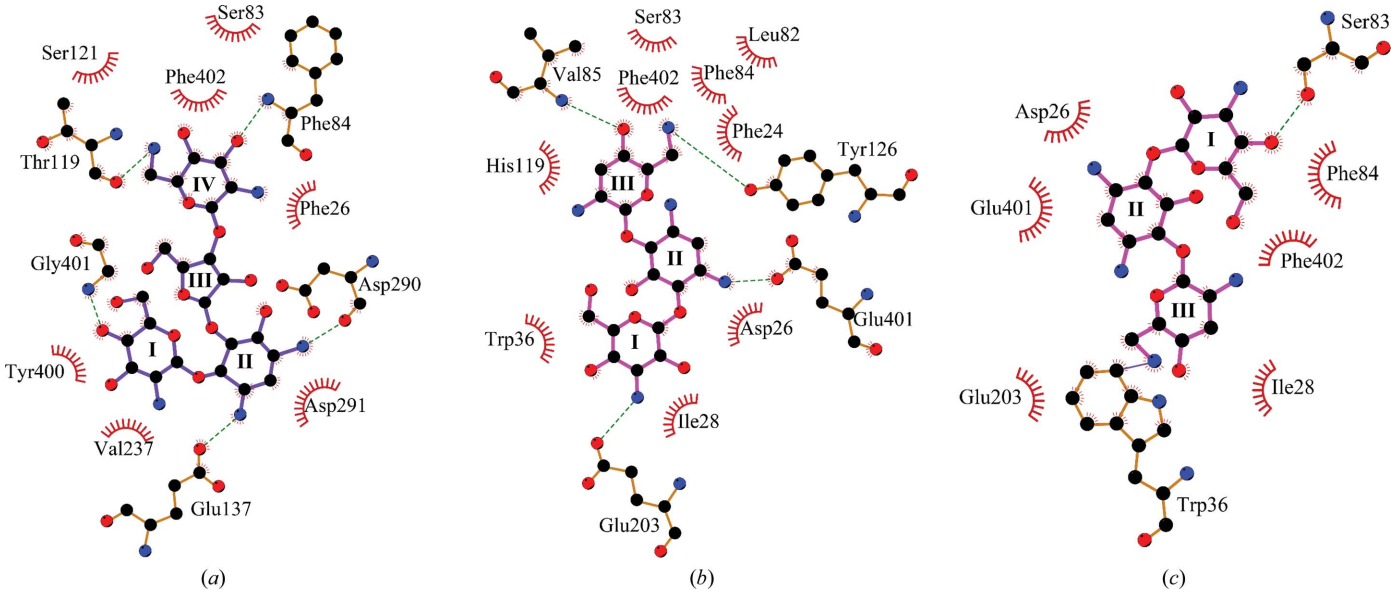

Figure 6
Interactions of aminoglycoside drugs with *Msm* Eis and *Mtb* Eis. (*a*) Paromomycin bound to *Msm* Eis (chain *A*). (*b*) Tobramycin bound to *Mtb* Eis (binding mode *A*; Houghton *et al.*, 2013). (*c*) Tobramycin bound to *Mtb* Eis (binding mode *B*; Houghton *et al.*, 2013). C, N and O atoms are coloured black, blue and red, respectively. The figure was prepared with *LigPlot+* (Laskowski & Swindells, 2011).

momycin. The absence of acetyl-CoA in the crystal may be owing to the presence of 1.26 *M* ammonium sulfate in the reservoir solution and/or to the absence of acetyl-CoA in the cryoprotectant solution.

3.3. Paromomycin binding to the *Msm* Eis active site

The six paromomycin molecules bound to the active sites of the *Msm* Eis hexamer in the asymmetric unit adopt essentially a single conformation in the crystal (Fig. 2 and Supplementary Fig. S1). *Msm* Eis was shown to triacetylate paromomycin (Chen *et al.*, 2012). It is not clear why the observed binding mode is preferred over other possible binding modes. In the observed binding mode, the side chain of Glu137 and the carbonyl group of Asp290 are hydrogen-bonded to two amines of paromomycin ring II, while the amino group of Gly401 interacts with the hydroxyl groups of ring I and ring III (Figs. 5*a* and 6*a*). Paromomycin ring IV is oriented by contacts with the backbone amino group of Phe84, the carbonyl group of Thr119 and the side chains of Ser121 and Phe402. Most residues of *Msm* Eis that interact with paromomycin are well conserved in *Mtb* Eis, except for Thr119, Glu137 and Gly401 of *Msm* Eis, which are replaced by His125, Leu143 and Glu407 in *Mtb* Eis (Supplementary Fig. S2).

Recently, a crystal structure of the *Mtb* Eis C204A mutant bound to tobramycin and CoA was reported at 3.5 Å resolution (Houghton *et al.*, 2013). Strong and continuous electron density for tobramycin was observed in two of the six aminoglycoside-binding pockets of the *Mtb* Eis hexamer in the asymmetric unit, and two possible binding modes (*A* and *B*) were modelled (Figs. 5*b*, 5*c*, 6*b* and 6*c*). This is in agreement with the finding that *Mtb* Eis (as well as *Msm* Eis) can acetylate multiple amines of several aminoglycosides (Chen *et al.*, 2012). The two binding modes are approximately related by a 180° rotation, a shift and a minor conformational change (Houghton *et al.*, 2013). Binding mode *A* is consistent with 6′-acetylation of tobramycin by *Mtb* Eis, while binding mode *B* is consistent with 3″-acetylation (Houghton *et al.*, 2013). The mode of paromomycin binding to *Msm* Eis is more similar to mode *A* of tobramycin binding to *Mtb* Eis. Rings III and IV of paromomycin and rings II and III of tobramycin are located at similar positions in the active sites of *Msm* Eis and *Mtb* Eis, respectively. As a consequence, the potential acetylation sites of paromomycin (the N64 atom) and tobramycin (the N61 atom) are located in highly similar positions (Fig. 4*b*). Rings III and IV of paromomycin are recognized by the active-site residues of *Msm* Eis in a manner somewhat similar to the recognition of rings II and III of tobramycin by the active-site residues of *Mtb* Eis (Figs. 5 and 6). Paromomycin rings III and IV are recognized by Phe26, Ser83, Phe84, Thr119, Ser121 and Phe402 of *Msm* Eis (Figs. 5*a* and 6*a*). Tobramycin rings II and III are recognized by Phe24, Leu82, Phe84, Val85, His119 and Phe402 of *Mtb* Eis in binding mode *A* (Figs. 5*b* and 6*b*). In mode *B* (Houghton *et al.*, 2013), tobramycin is recognized by Asp26, Ile28, Trp36, Ser83, Phe84, Glu203, Glu401 and Phe402 of *Mtb* Eis (Figs. 5*c* and 6*c*). It is hoped that our structural data on paromomycin-bound *Msm* Eis will be useful in the design of *Mtb* Eis inhibitors as novel antituberculosis antibiotics.

We thank the beamline staff at BL-5C and BL-7A of Pohang Light Source, Republic of Korea for assistance during X-ray diffraction experiments. This work was supported by the Korea Ministry of Science, ICT and Future Planning, the National Research Foundation of Korea (NRF-2013R1A2A1A05067303), the Innovative Drug Research Center for Metabolic and Inflammatory Disease and the Korea Ministry of Health, Welfare and Family Affairs (Korea Healthcare Technology R&D Project A092006).

References

Adams, P. D. *et al.* (2010). *Acta Cryst.* D**66**, 213–221.
Chen, V. B., Arendall, W. B., Headd, J. J., Keedy, D. A., Immormino, R. M., Kapral, G. J., Murray, L. W., Richardson, J. S. & Richardson, D. C. (2010). *Acta Cryst.* D**66**, 12–21.
Chen, W., Biswas, T., Porter, V. R., Tsodikov, O. V. & Garneau-Tsodikova, S. (2011). *Proc. Natl Acad. Sci. USA*, **108**, 9804–9808.
Chen, W., Green, K. D., Tsodikov, O. V. & Garneau-Tsodikova, S. (2012). *Biochemistry*, **51**, 4959–4967.
Chiang, C.-Y., Centis, R. & Migliori, G. B. (2010). *Respirology*, **15**, 413–432.
Dahl, J. L., Wei, J., Moulder, J. W., Laal, S. & Friedman, R. L. (2001). *Infect. Immun.* **69**, 4295–4302.
Dye, C. & Williams, B. G. (2010). *Science*, **328**, 856–861.
Emsley, P. & Cowtan, K. (2004). *Acta Cryst.* D**60**, 2126–2132.

Getahun, H., Gunneberg, C., Granich, R. & Nunn, P. (2010). *Clin. Infect. Dis.* **50**, S201–S207.
Houghton, J. L., Biswas, T., Chen, W., Tsodikov, O. V. & Garneau-Tsodikova, S. (2013). *Chembiochem*, **14**, 2127–2135.
Kim, K. H. *et al.* (2012). *Proc. Natl Acad. Sci. USA*, **109**, 7729–7734.
Laskowski, R. A. & Swindells, M. B. (2011). *J. Chem. Inf. Model.* **51**, 2778–2786.
Lella, R. K. & Sharma, C. (2007). *J. Biol. Chem.* **282**, 18671–18675.
Lin, P. L. & Flynn, J. L. (2010). *J. Immunol.* **185**, 15–22.
McCoy, A. J., Grosse-Kunstleve, R. W., Adams, P. D., Winn, M. D., Storoni, L. C. & Read, R. J. (2007). *J. Appl. Cryst.* **40**, 658–674.
Meena, L. S. & Rajni (2010). *FEBS J.* **277**, 2416–2427.
Murshudov, G. N., Skubák, P., Lebedev, A. A., Pannu, N. S., Steiner, R. A., Nicholls, R. A., Winn, M. D., Long, F. & Vagin, A. A. (2011). *Acta Cryst.* D**67**, 355–367.
Shin, D.-M., Jeon, B.-Y., Lee, H.-M., Jin, H. S., Yuk, J.-M., Song, C.-H., Lee, S.-H., Lee, Z.-W., Cho, S.-N., Kim, J.-M., Friedman, R. L. & Jo, E.-K. (2010). *PLoS Pathog.* **6**, e1001230.
Wei, J., Dahl, J. L., Moulder, J. W., Roberts, E. A., O'Gaora, P., Young, D. B. & Friedman, R. L. (2000). *J. Bacteriol.* **182**, 377–384.
Winn, M. D. *et al.* (2011). *Acta Cryst.* D**67**, 235–242.
Wu, S., Barnes, P. F., Samten, B., Pang, X., Rodrigue, S., Ghanny, S., Soteropoulos, P., Gaudreau, L. & Howard, S. T. (2009). *Microbiology*, **155**, 1272–1281.